

## EXTENDED Ly $\alpha$ EMISSION FROM INTERACTING GALAXIES AT HIGH REDSHIFTS

HIDENOBU YAJIMA<sup>1,2</sup>, YUEXING LI<sup>1,2</sup>, AND QIRONG ZHU<sup>1,2</sup>,

<sup>1</sup>Department of Astronomy & Astrophysics, The Pennsylvania State University, 525 Davey Lab, University Park, PA 16802, USA; yuh19@psu.edu and

<sup>2</sup>Institute for Gravitation and the Cosmos, The Pennsylvania State University, University Park, PA 16802, USA  
*Draft version August 31, 2017*

### ABSTRACT

Recent observations have discovered a population of extended Ly $\alpha$  sources, dubbed Ly $\alpha$  blobs (LABs), at high redshift  $z \sim 2-6.6$ . These LABs typically have a luminosity of  $L \sim 10^{42}-10^{44}$  erg s<sup>-1</sup>, and a size of tens of kiloparsecs, with some giant ones reaching up to  $D \sim 100$  kpc. However, the origin of these LABs is not well understood. In this paper, we investigate a merger model for the formation of LABs by studying Ly $\alpha$  emission from interacting galaxies at high redshifts by means of a combination of hydrodynamics simulations with three-dimensional radiative transfer calculations. Our galaxy simulations focus on a set of binary major mergers of galaxies with a mass range of  $3-7 \times 10^{12} M_{\odot}$  in the redshift range of  $z \sim 3-7$ , and we use the newly improved ART<sup>2</sup> code to perform the radiative transfer calculations which couple multi-wavelength continuum, ionization of hydrogen, and Ly $\alpha$  line emission. We find that intense star formation and enhanced cooling induced by gravitational interaction produce strong Ly $\alpha$  emission from these merging galaxies. The Ly $\alpha$  emission appears to be extended due to the extended distribution of sources and gas. During the close encounter of galaxy progenitors when the star formation rate peaks at  $\sim 10^3 M_{\odot} \text{ yr}^{-1}$ , our model produces LABs with luminosity of  $L \sim 10^{42}-10^{44}$  erg s<sup>-1</sup>, and size of  $D \sim 10-20$  kpc at  $z > 6$  and  $D \sim 20-50$  kpc at  $z \sim 3$ , in broad agreement with observations in the same redshift range. Our results suggest that merging galaxies may produce some typical LABs as observed, but the giant ones may be produced by mergers more massive than those in our model, or a combination of mergers and cold accretion from filaments on a large scale.

*Subject headings:* galaxies: high-redshift – galaxies: formation – galaxies: evolution – radiative transfer – hydrodynamics – methods: numerical

### 1. INTRODUCTION

Star formation in galaxies can produce strong Ly $\alpha$  line emission via recombination in HII region in the early phase of the evolution (Partridge & Peebles 1967; Charlot & Fall 1993). Recent narrow-band deep imaging surveys using large-aperture telescopes have detected a large population of Ly $\alpha$  emitting galaxies, generally called Ly $\alpha$  emitters (LAEs) when the equivalent width (EW) of the Ly $\alpha$  line is above 20 Å, at nearly all redshift up to  $z = 8.6$  (e.g., Cowie & Hu 1998; Hu et al. 1998; Malhotra & Rhoads 2004; Iye et al. 2006; Gronwall et al. 2007; Ouchi et al. 2010; Lehnert et al. 2010; Kashikawa et al. 2011; Shibuya et al. 2012). It is suggested that most LAEs are compact, young star-forming galaxies (e.g., Westra et al. 2005; Gawiser et al. 2007; Acquaviva et al. 2012, but see Kornei et al. 2010 for a different view).

Meanwhile, a number of extended and bright Ly $\alpha$  sources, which are called Ly $\alpha$  blobs (LABs), have also been discovered in the redshift range of  $z \sim 2-6.6$  (Keel et al. 1999; Steidel et al. 2000, 2011; Reuland et al. 2003; Palunas et al. 2004; Matsuda et al. 2004, 2011; Dey et al. 2005; Saito et al. 2006, 2008; Nilsson et al. 2006; Smith & Jarvis 2007; Prescott et al. 2008; Ouchi et al. 2009; Yang et al. 2009, 2010). These LABs have a luminosity in the range of  $\sim 10^{42}-10^{44}$  erg s<sup>-1</sup>, a size from tens of kiloparsecs up to  $\sim 100$  kpc, much more extended than the LAEs at the same redshift, and some LABs do not seem to have any optical

or infrared counterpart.

The origin of the LABs remains a hot debate. One proposal is that they may form from gravitational cooling radiation from accreting gas (Haiman et al. 2000; Fardal et al. 2001), motivated by the observations that some LABs lack visible power source in both optical and infrared (Nilsson et al. 2006; Smith et al. 2008). Recent hydrodynamics simulations show that galaxy evolution is accompanied by accretion of cold gas streams of  $T \sim 10^4-10^5$  K, which penetrate deep inside dark matter halos (Katz et al. 2003; Kereš et al. 2005, 2009; Birnboim & Dekel 2003; Dekel & Birnboim 2006; Ocvirk et al. 2008; Brooks et al. 2009; Dekel et al. 2009). Such inflow of cold gas may produce strong and extensive Ly $\alpha$  emission via collisional excitation, which may result in LABs if there is no dust absorption (Dijkstra & Loeb 2009; Faucher-Giguère et al. 2009; Goerdt et al. 2010; Yajima et al. 2012c).

However, other observations show that some LABs are associated with regular Lyman break galaxies (Matsuda et al. 2004), sub-millimeter and infrared sources which imply active star formation of  $\text{SFR} \sim 10^2-10^3 M_{\odot} \text{ yr}^{-1}$  (Chapman et al. 2001; Geach et al. 2005, 2007), or active galactic nuclei (AGN) and quasars (Bunker et al. 2003; Weidinger et al. 2004; Basu-Zych & Scharf 2004; Geach et al. 2007; Smith et al. 2009; Colbert et al. 2011). More recently, observations showed asymmetric, filamentary structure in some giant LABs (Matsuda et al. 2011; Erb et al. 2011; Rauch et al. 2011, 2013), which may result from

cold accretion or interaction-triggered inflow.

To explain the extended distribution of Ly $\alpha$  emission of LABs, stellar wind from supernovae feedback has been suggested as an effective mechanism (Taniguchi & Shioya 2000; Mori & Umemura 2006; Dijkstra & Kramer 2012). Mori & Umemura (2006) showed, by means of ultra-high resolution hydrodynamics simulations, that multiple supernovae feedbacks produced extended bubble structure and the compressed gas shell created numerous Ly $\alpha$  photons over extended region. However, it is not clear that triggers the starburst or AGN activity. In addition, most of the theoretical works assume that all Ly $\alpha$  photons can escape from the galaxy, but in reality, Ly $\alpha$  photons can experience numerous scattering and be absorbed by dust. Moreover, galactic wind is highly suppressed by gravitation potential at  $M_{\text{halo}} \gtrsim 10^{12} M_{\odot}$  (Springel 2005), which may not be effective in producing LABs.

In this work, we propose a formation model of LABs from major mergers of gas-rich galaxies. In such a merging process, strong gravitational torques create highly condensed gas clumps in the nuclei region and tidal tails, and trigger intense, global star formation (e.g., Hernquist 1989; Barnes & Hernquist 1992; Sanders & Mirabel 1996; Springel 2005; Hopkins et al. 2006). At higher redshift (e.g.,  $z \gtrsim 2$ ), the major merger rate is higher in dense regions and the progenitors are more gas rich (e.g., Li et al. 2007; Hopkins et al. 2010), which may produce strong, extended Ly $\alpha$  emission from both recombination of ionized gas and collisional excitation of neutral hydrogen (Yajima et al. 2012a,c,b). In fact, recent observations of LABs showed multiple star-forming clumps or galaxies in the regions (Colbert et al. 2006; Prescott et al. 2012; Uchimoto et al. 2012), which suggest a merger origin of these LABs.

To test this model, we investigate the Ly $\alpha$  property of interacting galaxies by combining hydrodynamical simulations with three dimensional radiative transfer (RT) calculations. The simulations follow the evolution of galaxy mergers of different mass and redshift, and the RT calculations uses the newly improved code ART<sup>2</sup> by Yajima et al. (2012a). The ART<sup>2</sup> code couples multi-wavelength continuum, Ly $\alpha$  line, and ionization of hydrogen, which is critical to study the Ly $\alpha$  and multi-band properties of galaxies.

The paper is organized as follows. We describe the galaxy simulations in §2, and the method of radiative transfer calculations in §3. In §4, we present the results of Ly $\alpha$  properties, which include the photon escape fraction, emergent Ly $\alpha$  luminosity, the EW, the line profile, Ly $\alpha$  surface brightness and the size. We discuss in §5 the effect of wind and AGN on the Ly $\alpha$  properties, and summarize in §6.

## 2. GALAXY MODEL

In order to determine the role mergers play in producing LABs, we perform a set of hydrodynamics simulations of binary, equal-mass, major mergers of galaxies. The galaxy is constructed based on the model of Mo et al. (1998), which consists of a dark matter halo, a disk of gas and stars, and a seed black hole of  $10^5 M_{\odot}$ , using a well-tested method (Hernquist 1993; Springel & White 1999; Springel 2000; Springel et al. 2005b). We follow the procedures of Li et al. (2007) to

generate the galaxy progenitors, the properties of which, including the virial mass  $M_{\text{vir}}$ , virial radius  $R_{\text{vir}}$  and halo concentration  $C_{\text{vir}}$ , are scaled appropriately with redshift.

$$M_{\text{vir}} = \frac{V_{\text{vir}}^3}{10GH(z)}, \quad (1)$$

$$R_{\text{vir}} = \frac{V_{\text{vir}}}{10H(z)}, \quad (2)$$

$$H(z) = H_0 [\Omega_{\Lambda} + (1 - \Omega_{\Lambda} - \Omega_{\text{m}})(1+z)^2 + \Omega_{\text{m}}(1+z)^3]^{1/2} \quad (3)$$

$$C_{\text{vir}} = 9 \left[ \frac{M_{\text{vir}}}{M_0} \right]^{-0.13} (1+z)^{-1}, \quad (4)$$

where  $G$  is the gravitational constant, and  $M_0 \sim 8 \times 10^{12} h^{-1} M_{\odot}$  is the linear collapse mass at the present epoch.

The density profile of the dark matter halo follows a Hernquist profile (Hernquist 1990), scaled to match that found in cosmological simulations (Navarro et al. 1997), as described in Springel (2005).

$$\rho(r) = \frac{M_{\text{vir}}}{2\pi} \frac{a}{r(r+a)^3}, \quad (5)$$

where  $a$  is a parameter that relates the Hernquist (1990) profile parameters to the appropriate Navarro-Frenk-White halo scale length  $R_s$  and concentration  $C_{\text{vir}}$  ( $C_{\text{vir}} = R_{\text{vir}}/R_s$ ),

$$a = R_s \sqrt{2[\ln(1 + C_{\text{vir}}) - C_{\text{vir}}/(1 + C_{\text{vir}})]}. \quad (6)$$

The exponential disk of stars and gas are then constructed as in Hernquist (1993) and Springel et al. (2005b). We assume a baryon fraction of  $f_b = 0.17$  for these high-redshift galaxies based on the seventh year *Wilkinson Microwave Anisotropy Probe* data (*WMAP7*; Komatsu et al. 2011). The gas fraction of each progenitor is extrapolated from the results of semi-analytical models of galaxy formation (Somerville et al. 2001), with 100% gas disks at  $z \geq 10$ , 90% at  $10 > z \gtrsim 6$ , and 60% at  $6 > z \gtrsim 4$ .

The simulations include dark matter, gasdynamics, star formation, black hole growth, and feedback processes, and are performed using the parallel,  $N$ -body/smoothed particle hydrodynamics (SPH) code GADGET-3, which is an improved version of that described in Springel et al. (2001); Springel (2005). GADGET implements the entropy-conserving formulation of SPH (Springel & Hernquist 2002) with adaptive particle smoothing, as in Hernquist & Katz (1989). Radiative cooling and heating processes are calculated assuming collisional ionization equilibrium (Katz et al. 1996; Davé et al. 1999). Star formation is modeled in a multi-phase interstellar medium (ISM), with a rate that follows the Schmidt-Kennicutt Law (Schmidt 1959; Kennicutt 1998). Feedback from supernovae is captured through a multi-phase model of the ISM by an effective equation of state for star-forming gas (Springel & Hernquist 2003). The UV background model of Haardt & Madau (1996) is used. A self-regulated black hole model is used, in which a spherical Bondi-Hoyle-Lyttleton gas accretion (Bondi 1952; Bondi & Hoyle 1944; Hoyle & Lyttleton

TABLE 1  
SIMULATION RUNS WITH DIFFERENT PARAMETERS AND FEEDBACK MODELS

Runs	$M_{\text{tot}} (M_{\odot})^{\text{a}}$	$z_{\text{init}}^{\text{b}}$	$N_{\text{DM}}^{\text{c}}$	$N_{\text{b}}^{\text{d}}$	BH	Wind	$f_{\text{gas}}^{\text{e}}$
z9A	$3 \times 10^{12}$	9	$6 \times 10^5$	$4 \times 10^5$	On	On	0.98
z6A	$5 \times 10^{12}$	6	$6 \times 10^5$	$4 \times 10^5$	On	On	0.9
z4.5A	$7 \times 10^{12}$	4.5	$6 \times 10^5$	$4 \times 10^5$	On	On	0.6
z4.5B	$7 \times 10^{12}$	4.5	$6 \times 10^5$	$4 \times 10^5$	Off	On	0.6
z4.5C ;	$7 \times 10^{12}$	4.5	$6 \times 10^5$	$4 \times 10^5$	On	Off	0.6

<sup>a</sup> Total mass of the merging system.

<sup>b</sup> Initial redshift of the simulation.

<sup>c</sup> Total number of dark matter particles.

<sup>d</sup> Total number of star and gas particles.

<sup>e</sup> Gas mass fraction to dark matter normalized by *WMAP-7* year data.

1941) with an upper limit of Eddington rate is assumed, and the feedback is in the form of thermal energy injected to the gas, as described in Springel et al. (2005a).

We also include a model of galactic wind driven by stellar feedback, as introduced by Springel & Hernquist (2003). We adopt a constant wind velocity of  $v_{\text{wind}} = 484 \text{ km s}^{-1}$ , a mass-loss rate that is twice of the star formation rate, and an energy efficiency of unity such that the wind carries 100% of the supernova energy. The wind direction is anisotropic, preferentially perpendicular to the galactic disk. This wind model causes an outflow of gas, transporting energy, matter and metals out of the galactic disk in proportion to the star formation rate (Springel & Hernquist 2003).

Table 1 lists the simulations performed in this work and the related physical and numerical parameters. The three fiducial runs, z9A, z6A, and z4.5A are set up to produce galaxy mergers at redshift  $z \sim 6, 4,$  and  $3,$  respectively, for direct comparison with observations. The progenitors of these mergers belong to the massive end at the given redshift. All these three simulations include thermal feedback from supernovae and black holes, and galactic wind. In order to investigate the effects of feedback on the Ly $\alpha$  properties of these merging systems, we also run two additional simulations, z4.5B and z4.5C, without black hole or wind, respectively. We adopt the cosmological parameters from the *WMAP7* results:  $H_0 = 72 \text{ km s}^{-1} \text{ Mpc}^{-1}$  ( $h = 0.72$ ),  $\Omega_M = 0.26$ ,  $\Omega_{\Lambda} = 0.74$ ,  $\Omega_b = 0.044$ ,  $\sigma_8 = 0.80$ , and  $n_s = 0.96$ .

### 3. RADIATIVE TRANSFER

The RT calculations are performed using the 3D Monte Carlo RT code, All-wavelength Radiative Transfer with Adaptive Refinement Tree (ART<sup>2</sup>), as recently developed by Yajima et al. (2012a). ART<sup>2</sup> was improved over the original version of Li et al. (2008), and features three essential modules: continuum emission from X-ray to radio, Ly $\alpha$  emission from both recombination and collisional excitation, and ionization of neutral hydrogen. The coupling of these three modules, together with an adaptive refinement grid, enables a self-consistent and accurate calculation of the Ly $\alpha$  properties, which depend strongly on the UV continuum, ionization structure, and dust content of the object. Moreover, it efficiently produces multi-wavelength properties, such as the spectral energy distribution and images, for direct comparison with multi-band observations. The detailed implementations of the ART<sup>2</sup> code are described in Li et al. (2008) and Yajima et al. (2012a). Here we focus on the Ly $\alpha$

calculations and briefly outline the process.

The Ly $\alpha$  emission is generated by two major mechanisms: recombination of ionizing photons and collisional excitation of hydrogen gas. In the recombination process, we consider ionization of neutral hydrogen by ionizing radiation from stars, active galactic nucleus (AGN), and UV background (UVB), as well as by collisions by high-temperature gas. The ionized hydrogen atoms then recombine and create Ly $\alpha$  photons via the state transition  $2\text{P} \rightarrow 1\text{S}$ . The Ly $\alpha$  emissivity from the recombination is

$$\epsilon_{\alpha}^{\text{rec}} = f_{\alpha} \alpha_{\text{B}} h \nu_{\alpha} n_{\text{e}} n_{\text{HII}}, \quad (7)$$

where  $\alpha_{\text{B}}$  is the case B recombination coefficient, and  $f_{\alpha}$  is the average number of Ly $\alpha$  photons produced per case B recombination. Here we use  $\alpha_{\text{B}}$  derived in Hui & Gnedin (1997). Since the temperature dependence of  $f_{\alpha}$  is not strong,  $f_{\alpha} = 0.68$  is assumed everywhere (Osterbrock & Ferland 2006). The product  $h \nu_{\alpha}$  is the energy of a Ly $\alpha$  photon, 10.2 eV.

In the process of collisional excitation, high temperature electrons can excite the quantum state of hydrogen gas by the collision. Due to the large Einstein A coefficient, the hydrogen gas can occur de-excitation with the Ly $\alpha$  emission. The Ly $\alpha$  emissivity by the collisional excitation is estimated by

$$\epsilon_{\alpha}^{\text{coll}} = C_{\text{Ly}\alpha} n_{\text{e}} n_{\text{HI}}, \quad (8)$$

where  $C_{\text{Ly}\alpha}$  is the collisional excitation coefficient,  $C_{\text{Ly}\alpha} = 3.7 \times 10^{-17} \exp(-h \nu_{\alpha} / kT) T^{-1/2} \text{ erg s}^{-1} \text{ cm}^3$  (Osterbrock & Ferland 2006).

Once the ionization structure have been determined, we estimate the intrinsic Ly $\alpha$  emissivity in each cell by the sum of above Ly $\alpha$  emissivity,  $\epsilon_{\alpha} = \epsilon_{\alpha}^{\text{rec}} + \epsilon_{\alpha}^{\text{coll}}$ .

In RT calculations, dust extinction from the ISM is included. The dust content is estimated according to the gas content and metallicity in each cell, which are taken from the hydrodynamic simulation. The dust-to-gas ratio of the Milky Way is used where the metallicity is of Solar abundance, and it is linearly interpolated for other metallicity. We use the stellar population synthesis model of GALAXEV (Bruzual & Charlot 2003) to produce intrinsic spectral energy distributions (SEDs) of stars for a grid of metallicity and age, and we use a simple, broken power law for the AGN (Li et al. 2008). A Salpeter (1955) initial mass function is used in our calculations.

We apply ART<sup>2</sup> to the above hydrodynamic merger simulations. In our post-processing procedure, we first calculate the RT of ionizing photons ( $\lambda \leq 912 \text{ \AA}$ ) and

estimate the ionization fraction of the ISM. The resulting ionization structure is then used to run the Ly $\alpha$  RT to derive the emissivity. Our fiducial run is done with  $N_{\text{ph}} = 10^5$  photon packets for each ionizing and Ly $\alpha$  components, which was demonstrated to show good convergence (Yajima et al. 2012a,c). The highest refinement of the adaptive grid corresponds to a cell size comparable to the spatial resolution of 20 pc in physical coordinate of the hydrodynamic simulation.

#### 4. Ly $\alpha$ PROPERTIES

The simulations z9A, z6A, and z4.5A produce mergers at redshift  $z \sim 6, 4$  and  $3$ , respectively. The high-redshift galaxy progenitors in our simulations are gas-rich and compact. The merging systems typically experience a series of separation, close encounter, and final coalescence phases. During the merging event, strong gravitational interactions between the progenitors lead to tidal tails, strong shocks and efficient gas inflow that triggers large-scale starbursts and fuels rapid accretion onto the black holes. Meanwhile, feedback from both supernovae and black holes suppress both star formation and black hole accretion. The resulting Ly $\alpha$  emission follows the evolution of the system, as illustrated in Figure 1 from the z4.5A run.

At  $t = 0.1$  Gyr after the simulation starts, the galaxy pair is undergoing the first close encounter. The Ly $\alpha$  emission extends to a large distance and shows two strong peaks around the two interacting nuclei. As the pair coalesces at  $t \sim 0.48 - 0.5$  Gyr, in contrast to a strong spike of starburst, the Ly $\alpha$  emission dims and shrinks, and shows holes in the central region of the system, indicating significant absorption. After that, the Ly $\alpha$  emission continues to decline and its distribution becomes more compact in the merger remnant.

Figure 2 shows the star formation history and the resulting Ly $\alpha$  properties of the three fiducial simulations, z9A, z6A, and z4.5A, respectively. Higher redshift system merges faster due to smaller dynamical time scale. All simulations show intense star formation during the merging process, which in general declines with time except a strong peak at the time of the final coalescence, with rates ranging from a few to  $\sim 10^3 M_{\odot} \text{ yr}^{-1}$ .

The majority of the Ly $\alpha$  photons are absorbed by dust in these merging systems. The escape fractions of Ly $\alpha$  photons,  $f_{\text{esc}}$ , are below 30%, and during the final coalescence phase, they fall to deep dips of  $f_{\text{esc}} \sim 1\%$ . This is caused by the sudden increase of absorption from the dust produced by the starburst, as well as a sudden increase of the scattering optical depth in the shocked and compressed gas regions. As a result, the Ly $\alpha$  luminosity declines with time, in particular, the z6A run shows a steep drop at the coalescence, even its SFR reaches  $\sim 3 \times 10^3 M_{\odot} \text{ yr}^{-1}$ . The z4.5A run generally has higher luminosity,  $L_{\text{Ly}\alpha} \sim 10^{42.7} - 10^{44.2} \text{ erg s}^{-1}$ , the z9A having  $L_{\text{Ly}\alpha} \sim 10^{41.7} - 10^{43.8} \text{ erg s}^{-1}$ , and z6A lies in between. The observed luminosity range of LABs in  $z \sim 3 - 6$  is  $\sim 10^{43} - 10^{44} \text{ erg s}^{-1}$ , within the range of our simulations.

The equivalent width (EW) of Ly $\alpha$  line is defined as the ratio of Ly $\alpha$  luminosity to the UV flux density at  $\gtrsim 1216\text{\AA}$ ,  $\text{EW} = L_{\text{Ly}\alpha}/f_{\text{UV}}$ , where  $f_{\text{UV}}$  is the mean flux from 1300  $\text{\AA}$  to 1600  $\text{\AA}$ . As shown in Figure 2, the EWs

of z4.5A run shows  $\sim 25 - 220\text{\AA}$ , while z9A has  $\sim 40 - 100\text{\AA}$ , and z6A  $\sim 50\text{\AA}$ . This range is in broad agreement with observations of EWs of LABs,  $\sim 40 - 200\text{\AA}$  (e.g., Saito et al. 2006).

From the three-dimensional Ly $\alpha$  map, we measure the size of the blob in a projected plane above a given flux limit. If the two galaxies are separated apart, we measure the size of the bigger one only. Figure 3 gives the size evolution of the Ly $\alpha$  blobs from the three fiducial simulations above  $2.2 \times 10^{-18} \text{ erg s}^{-1} \text{ cm}^{-2} \text{ arcsec}^{-2}$ , the detection threshold of Matsuda et al. (2004). The z4.5A run has a size in the range of  $D \sim 15 - 50$  kpc during the merging event, z6A in  $\sim 15 - 45$  kpc, and z9A in  $\sim 10 - 20$  kpc. These results are consistent with observations. For example, the most distant LAB detected at  $z = 6.6$  by Ouchi et al. (2009) has a luminosity  $L_{\text{Ly}\alpha} = 3.9 \times 10^{43} \text{ erg s}^{-1}$  and a size  $D \sim 17$  kpc, in good agreement with that in the z9A simulation, which represents a merger event in  $z \sim 6$ .

## 5. DISCUSSION

### 5.1. Effects of Galactic Wind and AGN Feedback

It has been suggested that stellar wind from supernovae or AGN feedback may produce the extended Ly $\alpha$  distribution of LABs (e.g., Taniguchi & Shioya 2000; Mori & Umemura 2006; Ouchi et al. 2010). To examine the effects of feedback on the formation of LABs, we compare simulations with and without feedback.

In our simulations, we adopt the supernovae feedback model from Springel & Hernquist (2003), and AGN feedback from Springel et al. (2005a). The feedback from supernovae includes both thermal and kinetic forms. The thermal energy is released to the surrounding ISM, which results in a multi-phase structure. The kinetic feedback is in form of an anisotropic galactic wind perpendicular to the galactic disk. The wind has a constant velocity of  $v_{\text{wind}} = 484 \text{ km s}^{-1}$ , a mass-loss rate that is twice of the star formation rate, and an energy efficiency of unity such that the wind carries 100% of the supernova energy. For the AGN feedback, about 5% of the radiated energy is injected to the gas thermally and isotropically, which would raise the gas temperature and cause an isotropic outflow.

Figure 4 shows a comparison of the LAB luminosity and size among simulations z4.5A (with both supernovae and AGN feedback), z4.5B (no AGN), and z4.5C (no wind, but with thermal feedback from both supernovae and AGN). While the feedback does not seem to affect significantly the resulting Ly $\alpha$  luminosity, the supernovae wind appears to make a remarkable difference in the Ly $\alpha$  distribution. Without wind, the Ly $\alpha$  is more concentrated, reducing the size by  $\sim 10\%$ . However, the AGN feedback does not seem have a significant effect on the Ly $\alpha$  distribution.

### 5.2. Velocity Width

Another important feature of LABs is the large velocity width ( $\Delta V$ ) of the Ly $\alpha$  lines. It was suggested that the LABs at  $z = 3.1$  from Matsuda et al. (2004) have a wide range of velocity width,  $\Delta V \sim 500 - 1700 \text{ km s}^{-1}$ , while the one detected at  $z = 6.6$  by Ouchi et al. (2009) has  $\Delta V \sim 250 \text{ km s}^{-1}$ .

Figure 5 shows the evolution of velocity width  $\Delta V$

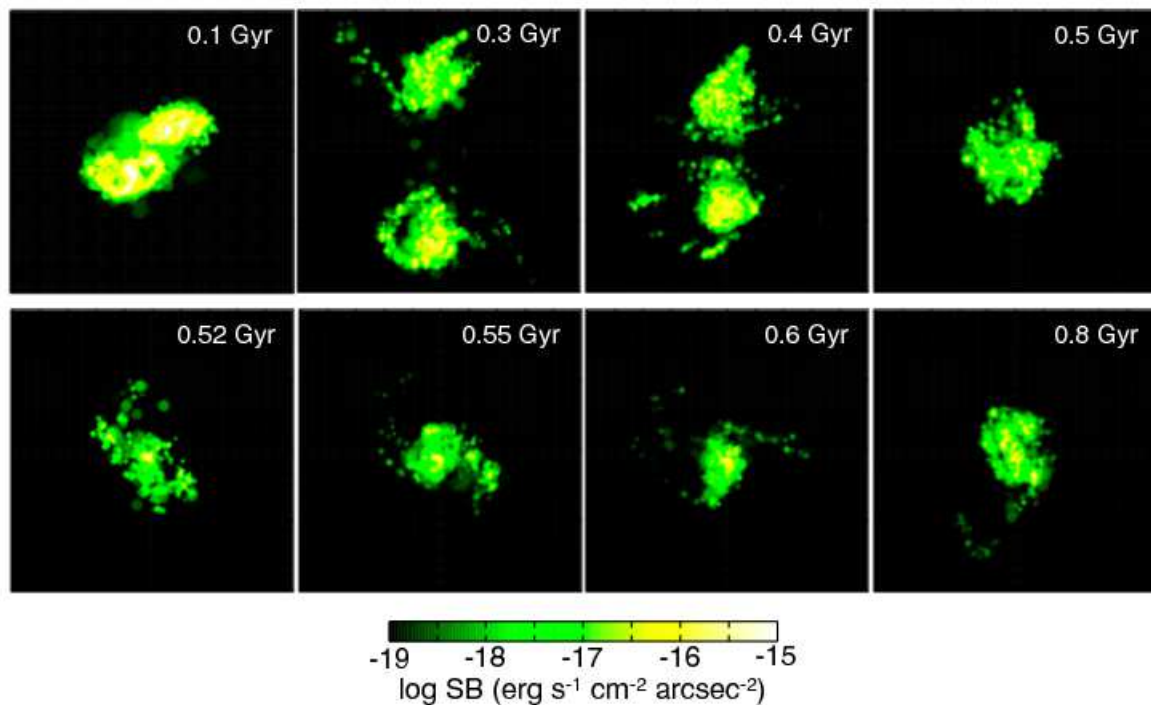


FIG. 1.— Evolution of the Ly $\alpha$  map during the merging event, from the z4.5A simulation. The box size is 100 kpc in physical scale, and the color bar indicates the surface brightness of the Ly $\alpha$  flux.

(measured by the FWHM of the Ly $\alpha$  line) from three simulations in our work. In all cases,  $\Delta V$  changes significantly with time as the interacting galaxies evolve dynamically. During the merging process, large velocity width is expected when the two progenitors approach to each other, it then drops after the encounter. After the coalescence, large  $\Delta V$  may be maintained by the rotational motion of gas and the wind feedback due to the active star formation. In the plot, the peak of z9A run (blue line) corresponds to the snapshot right before the first encounter, while the dip of the z6A case (green line) corresponds to a time shortly after the first passage. Overall, our simulations show a range of  $\Delta V \sim 100 - 1100 \text{ km s}^{-1}$  in these galaxy mergers. This range agrees well with the observations, which suggests that the large velocity width seen in some LABs may be caused by galaxy interactions.

### 5.3. Limitations of Our Model

In this work, the galaxy mergers are idealized and are simulated in isolation. The mergers constructed at different redshifts show consistent Ly $\alpha$  properties. However, in a cosmological context, galaxies at different redshift and environment may have different properties such as geometry, metallicity and dust content, which would significantly affect the Ly $\alpha$  properties.

In observation, LABs appear more common at high redshifts ( $z \sim 3 - 6.6$ ). While some are detected around  $z \sim 2$  (Palunas et al. 2004; Yang et al. 2009, 2010; Prescott et al. 2012), it is rare to find LABs at lower redshift  $z < 1$  (e.g., Keel et al. 2009). In our work, however, since we focus on isolated mergers, we cannot produce a redshift distribution of LABs. Furthermore, while our model can produce luminous ( $L_{\text{Ly}\alpha} \sim 10^{43} - 10^{44} \text{ erg s}^{-1}$ ) and extended ( $D \sim 20 - 50 \text{ kpc}$ ) Ly $\alpha$  sources at  $z \sim 3$  by idealized, binary major mergers, they fall short to reproduce the observed giant LABs with a size of  $\sim 100 \text{ kpc}$  (Matsuda et al. 2004, 2011). These giant LABs may form from mergers more massive than the ones we modeled, or from multiple mergers, or from a combination of mergers and accretion of cold gas along the filaments on a large scale.

In a cold dark matter cosmology, galaxies form hierarchically, with small objects collapsing first and subsequently merging to form progressively more massive ones. In this picture, massive galaxies form in high overdensity regions where mergers occur frequently (Li et al. 2007). The merging event may occur along the filamentary structure of intergalactic medium, and may be accompanied by accretion of cold gas onto the galaxy from the filaments. In these cases, the Ly $\alpha$  emission may have very extensive distribution due to scattering along the

cold flows and filaments.

To systematically investigate the formation of LABs, an ideal approach would be to combine multi-wavelength radiative transfer calculations, as those presented here, with full cosmological simulations which follow galaxy formation and evolution at different cosmic epochs. Such large-scale simulations, however, typically lack the high resolutions required to resolve the Ly $\alpha$  emission. We will tackle this issue in future work.

## 6. SUMMARY

By combining hydrodynamical simulations of interacting galaxies and radiative transfer calculations, we investigate the possibility of producing extended Ly $\alpha$  blobs from binary, major mergers. We focus on three mergers taking place in the redshift range of  $z \sim 3-7$  with a mass range of  $3-7 \times 10^{12} M_{\odot}$ . We find that the highly shocked gas regions and intense star formation induced by the gravitational interaction produce strong Ly $\alpha$  emission from these merging galaxies. The Ly $\alpha$  emission appear to be extended due to the extended distribution of sources and gas. It has a luminosity of  $L \sim 10^{43} - 10^{44} \text{ erg s}^{-1}$  and a size of  $D \sim 10 - 20 \text{ kpc}$  at  $z > 6$ ,  $D \sim 20 - 50 \text{ kpc}$  at  $z \sim 3$ . These results are in good agreement with observations of typical Ly $\alpha$  blobs from redshift  $z \sim 3$  to 6.6. Furthermore, we find that feedback from supernovae or AGN does not have a significant impact on the Ly $\alpha$  flux, but the presence of galactic wind from supernovae appear to increase the size of the blobs by  $\sim 10\%$ .

We note that our model does not produce giant Ly $\alpha$

blobs of  $\sim 100 \text{ kpc}$ . This suggests that giant LABs may form from mergers more massive than the ones we presented here, or from multiple mergers, or from a combination of mergers and cold accretion along the filaments on a large scale. To fully account for the Ly $\alpha$  sources in these scenarios, one needs to combine high-resolution cosmological hydrodynamics simulations of galaxy formation and evolution, with three-dimensional radiative transfer calculations, which we plan to investigate in a forthcoming paper.

We thank Tom Abel, Mark Dijkstra, Claude-André Faucher-Giguère, Eric Gawiser, Caryl Gronwall, Robin Ciardullo and Lars Hernquist for stimulating discussions and helpful comments. We thank the referee for constructive suggestions which have helped improve the manuscript. Support from NSF grants AST-0965694 and AST-1009867 is gratefully acknowledged. YL thanks the Institute for Theory and Computation (ITC) at Harvard University where the project was started for warm hospitality. We acknowledge the Research Computing and Cyberinfrastructure unit of Information Technology Services at The Pennsylvania State University for providing computational resources and services that have contributed to the research results reported in this paper (URL: <http://rcc.its.psu.edu>). The Institute for Gravitation and the Cosmos is supported by the Eberly College of Science and the Office of the Senior Vice President for Research at the Pennsylvania State University.

## REFERENCES

- Acquaviva, V., Vargas, C., Gawiser, E., & Guaita, L. 2012, *ApJL*, 751, L26
- Barnes, J. E. & Hernquist, L. 1992, *Natur*, 360, 715
- Basu-Zych, A. & Scharf, C. 2004, *ApJL*, 615, L85
- Birnboim, Y. & Dekel, A. 2003, *MNRAS*, 345, 349
- Bondi, H. 1952, *MNRAS*, 112, 195
- Bondi, H. & Hoyle, F. 1944, *MNRAS*, 104, 273
- Brooks, A. M., Governato, F., Quinn, T., Brook, C. B., & Wadsley, J. 2009, *ApJ*, 694, 396
- Bruzual, G. & Charlot, S. 2003, *MNRAS*, 344, 1000
- Bunker, A., Smith, J., Spinrad, H., Stern, D., & Warren, S. 2003, *Ap&SS*, 284, 357
- Chapman, S. C., Lewis, G. F., Scott, D., et al. 2001, *ApJL*, 548, L17
- Charlot, S. & Fall, S. M. 1993, *ApJ*, 415, 580
- Colbert, J. W., Teplitz, H., Francis, P. et al. 2006, *ApJ*, 637, L89
- Colbert, J. W., Scarlata, C., Teplitz, H., et al. 2011, *ApJ*, 728, 59
- Cowie, L. L. & Hu, E. M. 1998, *AJ*, 115, 1319
- Davé, R., Hernquist, L., Katz, N., & Weinberg, D. H. 1999, *ApJ*, 511, 521
- Dekel, A. & Birnboim, Y. 2006, *MNRAS*, 368, 2
- Dekel, A., Birnboim, Y., Engel, G., et al. 2009, *Natur*, 457, 451
- Dey, A., Bian, C., Soifer, B. T., et al. 2005, *ApJ*, 629, 654
- Dijkstra, M. & Loeb, A. 2009, *MNRAS*, 400, 1109
- Dijkstra, M. & Kramer, R. 2012, *MNRAS*, 424, 1672
- Erb, D. K., Bogosavljevic, M., & Steidel, C. C. 2011, *ApJ*, 740, L31
- Fardal, M. A., Katz, N., Gardner, J. P., et al. 2001, *ApJ*, 562, 605
- Faucher-Giguère, C., Lidz, A., Zaldarriaga, M., & Hernquist, L. 2009, *ApJ*, 703, 1416
- Gawiser, E., Francke, H., Lai, K., et al. 2007, *ApJ*, 671, 278
- Geach, J. E., Matsuda, Y., Smail, I., et al. 2005, *MNRAS*, 363, 1398
- Geach, J. E., Smail, I., Chapman, S. C., et al. 2007, *ApJL*, 655, L9
- Goerdt, T., Dekel, A., Sternberg, A., et al. 2010, *MNRAS*, 407, 613
- Gronwall, C., Ciardullo, R., Hickey, T., et al. 2007, *ApJ*, 667, 79
- Haardt, F. & Madau, P. 1996, *ApJ*, 461, 20
- Haiman, Z., Spaans, M., & Quataert, E. 2000, *ApJL*, 537, L5
- Hernquist, L. 1989, *Natur*, 340, 687
- Hernquist, L. 1990, *ApJ*, 356, 359
- Hernquist, L. 1993, *ApJS*, 86, 389
- Hernquist, L. & Katz, N. 1989, *ApJS*, 70, 419
- Hopkins, P. F., Bundy, K., Croton, D., et al. 2010, *ApJ*, 715, 202
- Hopkins, P. F., Hernquist, L., Cox, T. J., et al. 2006, *ApJS*, 163, 1
- Hoyle, F. & Lyttleton, R. A. 1941, *MNRAS*, 101, 227
- Hu, E. M., Cowie, L. L., & McMahon, R. G. 1998, *ApJ*, 502, L99+
- Hui, L. & Gnedin, N. Y. 1997, *MNRAS*, 292, 27
- Iye, M., Ota, K., Kashikawa, N., et al. 2006, *Natur*, 443, 186
- Kashikawa, N., Shimasaku, K., Matsuda, Y., et al. 2011, *ApJ*, 734, 119
- Katz, N., Keres, D., Dave, R., & Weinberg, D. H. 2003, in *Astrophysics and Space Science Library*, Vol. 281, The IGM/Galaxy Connection. The Distribution of Baryons at  $z=0$ , ed. J. L. Rosenberg & M. E. Putman, 185+.
- Katz, N., Weinberg, D. H., Hernquist, L., & Miralda-Escude, J. 1996, *ApJ*, 457, L57+
- Keel, W. C., Cohen, S. H., Windhorst, R. A., & Waddington, I. 1999, *AJ*, 118, 2547
- Keel, W. C., White, R. E., III, Chapman, S., & Windhorst, R. A. 2009, *AJ*, 138, 986
- Kennicutt, Jr., R. C. 1998, *ARA&A*, 36, 189
- Kereš, D., Katz, N., Fardal, M., Davé, R., & Weinberg, D. H. 2009, *MNRAS*, 395, 160
- Kereš, D., Katz, N., Weinberg, D. H., & Davé, R. 2005, *MNRAS*, 363, 2
- Komatsu, E., Smith, K. M., Dunkley, J., et al. 2011, *ApJS*, 192, 18
- Kornei, K. A., Shapley, A. E., Erb, D. K., et al. 2010, *ApJ*, 711, 693
- Lehnert, M. D., Nesvadba, N. P. H., Cuby, J., et al. 2010, *Natur*, 467, 940
- Li, Y., Hernquist, L., Robertson, B., et al. 2007, *ApJ*, 665, 187
- Li, Y., Hopkins, P. F., Hernquist, L., et al. 2008, *ApJ*, 678, 41

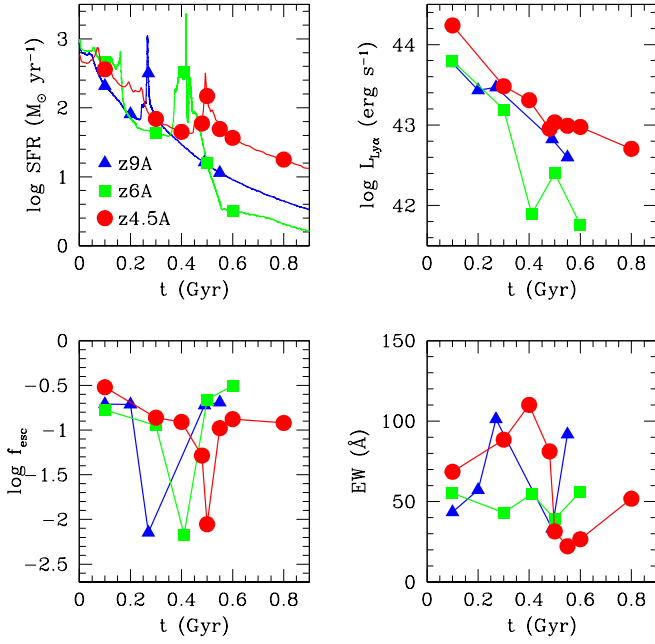


FIG. 2.— Evolution of the physical and Ly $\alpha$  properties during the galaxy mergers from the three fiducial simulations, z9A, z6A, and z4.5A, which produce an merging event at  $z \sim 6, 4,$  and  $3,$  respectively. From top to bottom in clockwise direction are: the star formation rate (upper left panel), the emergent Ly $\alpha$  luminosity (upper right), the equivalent width of Ly $\alpha$  line (lower right), and the escape fraction of Ly $\alpha$  photons (lower left).

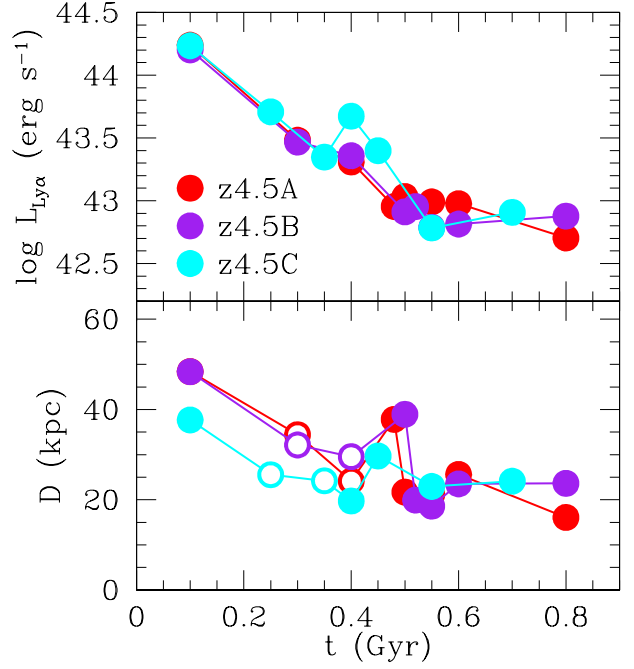


FIG. 4.— Comparison of the luminosity (*upper*) and size (*lower*) from simulations with different feedback schemes: z4.5A (red, includes both supernovae wind and AGN feedback), z4.5B (purple, no AGN), and z4.5C (cyan, no wind). Similar to Figure 3, the flux limit for deriving the size is  $2.2 \times 10^{-18} \text{ erg s}^{-1} \text{ cm}^{-2} \text{ arcsec}^{-2}$ , and the filled symbols indicate that the Ly $\alpha$  blobs from progenitors are overlapping, while open symbols indicate that they are separated, and that the size refers to the bigger blob only.

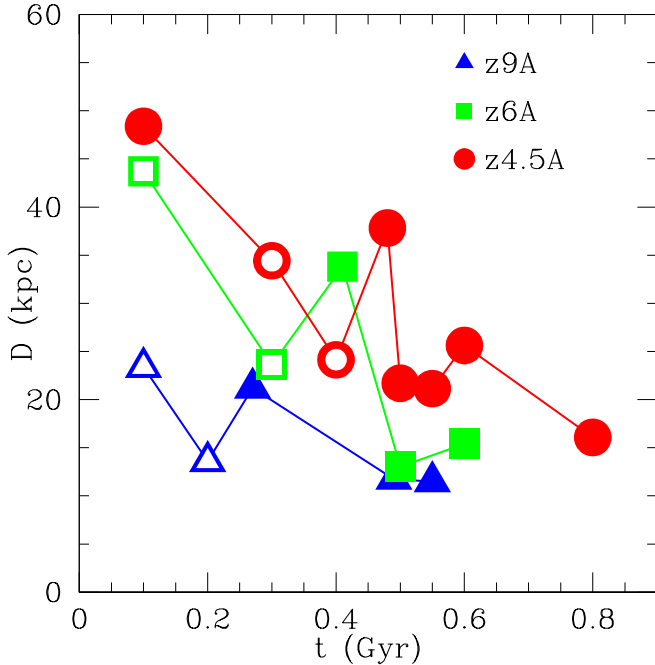


FIG. 3.— A comparison of the size of LABs above the detection limit from the three fiducial simulations, z9A, z6A, and z4.5A. The flux limit is  $2.2 \times 10^{-18} \text{ erg s}^{-1} \text{ cm}^{-2} \text{ arcsec}^{-2}$  from Matsuda et al. (2004). During the merging events, the Ly $\alpha$  emission from the two progenitors sometimes overlaps (indicated by filled symbols) and sometimes separates apart (indicated by open symbols). In the separation phase, the size refers to the bigger blob only.

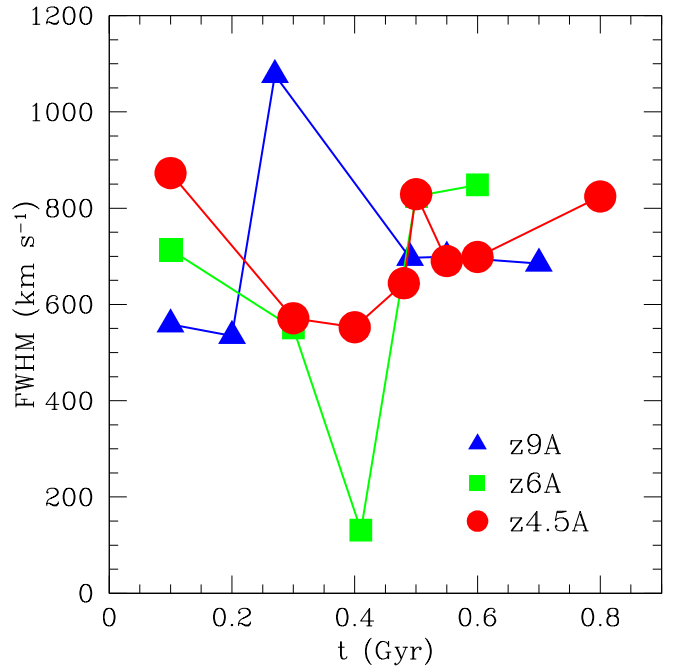


FIG. 5.— The evolution of velocity width of the Ly $\alpha$  line of three different merging systems in our simulations. The velocity width is measured by the Full Width of Half Maximum (FWHM) of the emergent Ly $\alpha$  line.

- Malhotra, S. & Rhoads, J. E. 2004, *ApJL*, 617, L5
- Matsuda, Y., Yamada, T., Hayashino, T., et al. 2004, *AJ*, 128, 569
- Matsuda, Y., Yamada, T., Hayashino, T., et al. 2011, *MNRAS*, 410, L13
- Mo, H. J., Mao, S., & White, S. D. M. 1998, *MNRAS*, 295, 319
- Mori, M. & Umemura, M. 2006, *Natur*, 440, 644
- Navarro, J. F., Frenk, C. S., & White, S. D. M. 1997, *ApJ*, 490, 493
- Nilsson, K. K., Fynbo, J. P. U., Møller, P., Sommer-Larsen, J., & Ledoux, C. 2006, *A&A*, 452, L23
- Ocvirk, P., Pichon, C., & Teyssier, R. 2008, *MNRAS*, 390, 1326
- Osterbrock, D. E. & Ferland, G. J. (ed.) 2006, *Astrophysics of Gaseous Nebulae and Active Galactic Nuclei* (Sausalito, CA: Univ. Science Books)
- Ouchi, M., Ono, Y., Egami, E., et al. 2009, *ApJ*, 696, 1164
- Ouchi, M., Shimasaku, K., Furusawa, H., et al. 2010, *ApJ*, 723, 869
- Palunas, P., Teplitz, H. I., Francis, P. J., Williger, G. M., & Woodgate, B. E. 2004, *ApJ*, 602, 545
- Partridge, R. B. & Peebles, P. J. E. 1967, *ApJ*, 147, 868
- Prescott, M. K. M., Kashikawa, N., Dey, A., & Matsuda, Y. 2008, *ApJL*, 678, L77
- Prescott, M. K. M., Dey, A., Brodwin, M., et al. 2012, *ApJ*, 752, 86
- Rauch, M., Becker, G. D., Haehnelt, M. G., et al. 2011, *MNRAS*, 418, 1115
- Rauch, M., Becker, G. D., Haehnelt, M. G., Gauthier, J.-R., & Sargent, W. L. W. 2013, *MNRAS*, 429, 429
- Reuland, M., van Breugel, W., Röttgering, H., et al. 2003, *ApJ*, 592, 755
- Saito, T., Shimasaku, K., Okamura, S., et al. 2006, *ApJ*, 648, 54
- Saito, T., Shimasaku, K., Okamura, S., et al. 2008, *ApJ*, 675, 1076
- Salpeter, E. E. 1955, *ApJ*, 121, 161
- Sanders, D. B. & Mirabel, I. F. 1996, *ARA&A*, 34, 749
- Schmidt, M. 1959, *ApJ*, 129, 243
- Shibuya, T., Kashikawa, N., Ota, K., et al. 2012, *ApJ*, 752, 114
- Smith, D. J. B. & Jarvis, M. J. 2007, *MNRAS*, 378, L49
- Smith, D. J. B., Jarvis, M. J., Lacy, M., & Martínez-Sansigre, A. 2008, *MNRAS*, 389, 799
- Smith, D. J. B., Jarvis, M. J., Simpson, C., & Martínez-Sansigre, A. 2009, *MNRAS*, 393, 309
- Somerville, R. S., Primack, J. R., & Faber, S. M. 2001, *MNRAS*, 320, 504
- Springel, V. 2000, *MNRAS*, 312, 859
- Springel, V. 2005, *MNRAS*, 364, 1105
- Springel, V., Di Matteo, T., & Hernquist, L. 2005a, *ApJL*, 620, L79
- Springel, V., Di Matteo, T., & Hernquist, L. 2005b, *MNRAS*, 361, 776
- Springel, V. & Hernquist, L. 2002, *MNRAS*, 333, 649
- Springel, V. & Hernquist, L. 2003, *MNRAS*, 339, 289
- Springel, V. & White, S. D. M. 1999, *MNRAS*, 307, 162
- Springel, V., Yoshida, N., & White, S. D. M. 2001, *NewA*, 6, 79
- Steidel, C. C., Adelberger, K. L., Shapley, A. E., et al. 2000, *ApJ*, 532, 170
- Steidel, C. C., Bogosavljević, M., Shapley, A. E., et al. 2011, *ApJ*, 736, 160
- Taniguchi, Y. & Shioya, Y. 2000, *ApJ*, 532, L13
- Uchimoto, Y. K., Yamada, T., Kajisawa, M., et al. 2012, *ApJ*, 750, 116
- Weidinger, M., Møller, P., & Fynbo, J. P. U. 2004, *Nature*, 430, 999
- Westra, E., Jones, D. H., Lidman, C. E., et al. 2005, *A&A*, 430, L21
- Yajima, H., Li, Y., Zhu, Q., & Abel, T. 2012a, *MNRAS*, 424, 884
- Yajima, H., Li, Y., Zhu, Q., et al. 2012b, arXiv: 1209.5842
- Yajima, H., Li, Y., Zhu, Q., et al. 2012c, *ApJ*, 754, 118
- Yang, Y., Zabludoff, A., Eisenstein, D., & Davé, R. 2010, *ApJ*, 719, 1654
- Yang, Y., Zabludoff, A., Tremonti, C., Eisenstein, D., & Davé, R. 2009, *ApJ*, 693, 1579